Advanced Integration of Safeguards Measurements

Philip Lafreniere[1], Mike Fugate[1], and Brian Key[1]

[1]Los Alamos National Laboratory

P.O Box 1663

Los Alamos, NM 87545

Abstract

Advanced integration efforts for safeguards were applied to assist the development of the Virtual Facility Distributed Test Bed (VFDTB). The sensor modeling work in this paper assisted both the safeguards and security modeling work for a pyroprocessing facility as part of the VFDTB. Sensor data and statistical analysis was integrated into a three-dimensional facility model and the Separation and Safeguards Performance Model (SSPM). To assist the development of the three-dimensional facility model, a pyroprocessing process hot cell was modeled in Monte Carlo N-Particle Code (MCNP) to map both its gamma and neutron radiation field with time. This model was comprised of simplified models of pyroprocessing equipment and utilized radiation source terms calculated from mass movement data from the SSPM. This work also helped inform the SSPM through MCNP modeling of the high dose neutron detector (HDND) and a microcalorimeter detector both developed at Los Alamos National Laboratory (LANL). The modeling examined the measurement and detection of the diversion of special nuclear material (SNM) in a pyroprocessing uranium product ingot. In addition to ingot counting, the HDND model was simulated in the hot cell model to determine potential radiation signatures that could be monitored to generate conclusions about the movement of material with time and to calculate background radiation in the hot cell. The results of the hot cell mapping and the assessment of the ingot for both neutron and gammas are presented in this paper.

Introduction

The United States Department of Energy's (US-DOE) Material Protection, Accounting, and Control Technologies (MPACT) campaign has developed a Virtual Facility Distributed Test Bed (VFDTB) to demonstrate safeguards and security by design (SSBD) as applied to a pyroprocessing facility. Safeguards modeling is performed using the Separation and Safeguards Performance Model (SSPM) from Sandia National Laboratory (SNL).[1] The SSPM models the facility's movement of mass with associated safeguards measurements at various unit operations.

In addition, the model integrates information related to process monitoring to increase the safeguards measurement confidence.

The advanced integration work described here was performed at Los Alamos National Laboratory (LANL) which consisted of simulating various safeguard sensors applied to different unit operations in the process. These simulations produced data that was further analyzed with advanced statistics to determine safeguards-related factors such as sensor deployment and probability of detection for diversions. The data and conclusions were then integrated into the SSPM to allow greater fidelity of its conclusions regarding the safeguards system design of the facility. The work has focused primarily on radiation counting for both neutrons and gammas. LANL simulated the High Dose Neutron Detector (HDND) for the neutron counts and the microcalorimeter for the gamma counts.[2,3]

This paper provides background regarding the advanced integration methods; the sensor simulation and statistical analysis campaigns undertaken to assist the integration framework. It then details the models developed and their methodology for its application to advanced integration. Results are then presented for the simulations and statistical testing. Finally, high level conclusions regarding what is to best be integrated into the VFDTB are provided.

Background

The advanced integration approach deployed follows the general method seen in the flow diagram in Figure 1. The first step is sensor simulation. Multiple simulation campaigns were undertaken as part of this step and are the focus of this paper. The first campaign was the development of pyroprocessing hot cell flux profiles for both neutron and gamma flux to determine the nature of the background radiation throughout the hot cell. The second campaign was neutron measurements of uranium (U) and uranium/transuranic (U/TRU) ingot in-situ in the hot cell given information for background neutron flux. The third campaign involved gamma spectra modeling for different sample unit operations and products.

The data collected by these campaigns was then integrated into models such as the SSPM and physical layout models. In addition to being calculated for integration directly into the models, the data was also further analyzed using statistical methods to determine factors such as probability of detection of diversion. These types of analyses differed based on the type of signal being interpreted, such as a bulk neutron count of a U ingot or the gamma spectra of a sample salt. Based off these analyzed results, this data was interpreted further for conclusions regarding which instruments are desirable for certain applications, what method or arrangement of sensors allows for a higher probability of detection, or what approach may lead to a greater number of false alarms. Conclusions based off these interpretations are also integrated into the safeguards model. This integration of statistical conclusions and data provides safeguards measurement information for the SSPM model at a level of fidelity above simple assumptions or Nondestructive Assay (NDA) measurement goals.[1]

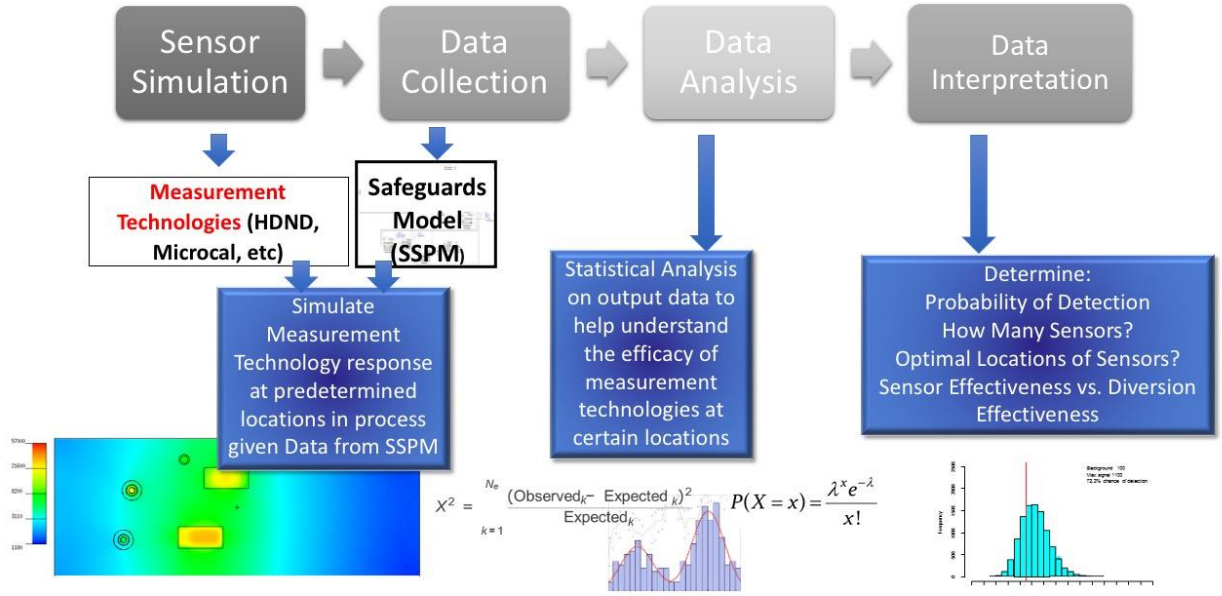

Figure 1. Advanced integration flowsheet

In order to perform proper sensor simulations for integration into the SSPM, the SSPM provided the physical material data to be interpreted by the sensor simulations therefore producing a reciprocal relationship for the SSPM and the advanced integration sensor modeling campaigns. The SSPM provided data for materials of both output products and the materials within the various unit operations. This material information was then integrated into the hot cell and sensor modeling to provide the desired safeguards data and conclusions. The relevant areas for the SSPM where sensor simulation was used to produce data for integration are seen in Figure 2. Gamma spectroscopy modeling was performed using data from the input spent nuclear fuel and electrorefiner salt to identify signatures of diversion. For the U and U/TRU products from the processors, simulations were undertaken for both neutron and gamma measurements to determine which sensor methods were most applicable. Each unit operation's mass data for MBA 2 in the SSPM created the material information for the background neutron and gamma sources calculated in the pyroprocessing hot cell model.

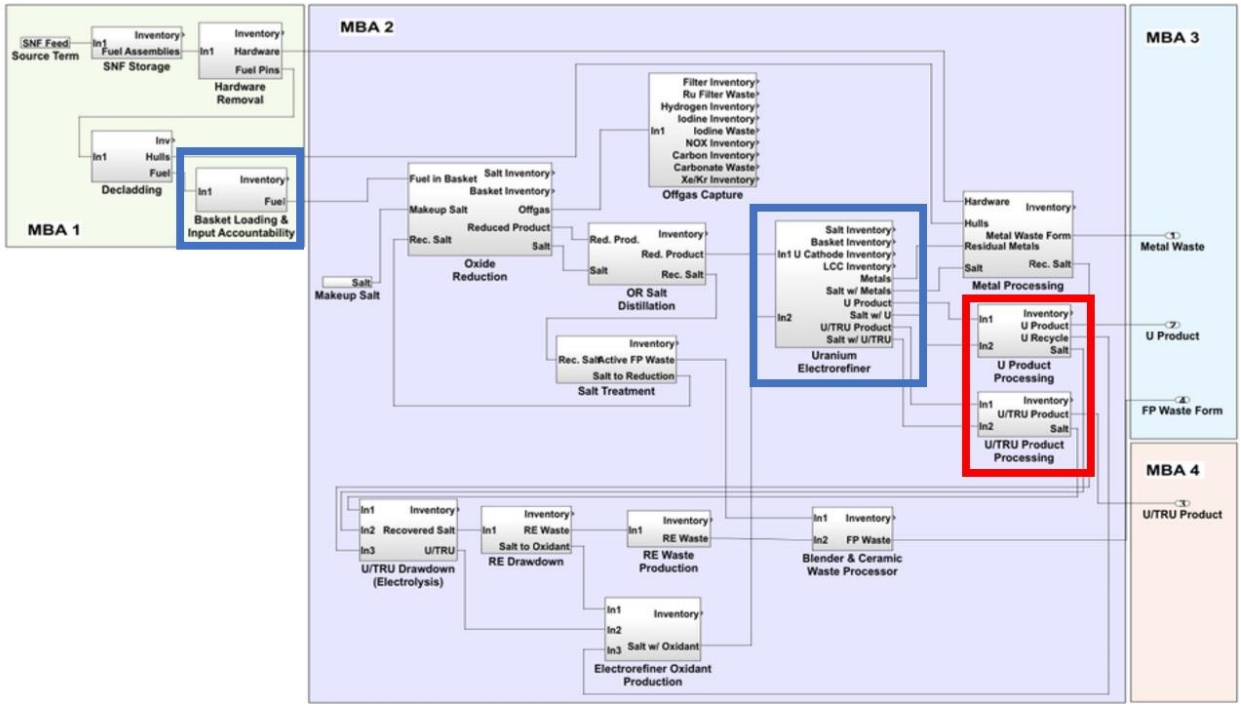

Figure 2. SSPM flowsheet, boxes represent locations of advanced integration measurements

For the neutron and gamma measurements, two specific technologies were modeled to produce the safeguards relevant data. For neutron measurements, the High Dose Neutron Detector (HDND) was the modeling focus.[2] The HDND, developed at LANL, is designed specifically for these types of high background applications. It consists of a series of boron lined tubes filled with carbon gas that measures pulses from captures in the boron lining.

For gamma spectrum measurements and analysis, the microcalorimeter detector, also developed by LANL, was simulated for a variety of applications.[3] The microcalorimeter is a gamma detector that measures changes in temperature in small thermal volumes utilizing cryogenics. This allows for high energy detection resolution in the low gamma energy range (<300 keV) with a precision of resolution on the scale of 10 eV. The detector consists of 288 tin absorbers with a volume of about 1 mm^3 per piece cooled using cryogenics to ensure that tiny changes in temperature are detected. These absorbers act as the detector's sensitive media.

To achieve these goals, a number of different models and modeling codes were used to calculate the modeled data and perform statistical analysis upon it. For both the pyroprocessing process equipment and U ingot,[4,5,6] the data from Echem-SSPM was used to develop materials to calculate neutron source terms using SOURCES-4C. The gamma sources were calculated using the Multiple Isotope Source Calculator (MISC) in the Monte Carlo N-Particle Code Tools suite (MCNPTools). An MCNP model of the pyroprocessing cell was generated to calculate the background neutron count rate for a modeled HDND at various positions throughout the cell using the neutron source term for the pyroprocessing process equipment. In addition to the background count rate, a counting model was developed for the U and U/TRU ingot using the same MCNP model of the HDND. A model of the microcalorimeter in GEANT4 was used to study the detector response in the 0-300 keV range using a point source term for a sampled U

ingot for the gamma spectrum of the ingot calculated in MISC.[7] These response terms, with the neutron background factored into HDND response, had statistical analysis performed to determine probability of detection of material diversion. These probabilities of detection were then integrated into the Echem-SSPM model to examine how these numbers affect the probability of detection of diversion across the entire flowsheet of the facility. A flowsheet of how these individual models inform one another is seen in Figure 3. The focus of this paper is on the advanced integration of the measurement simulations and determination of the probability of detection to be integrated into the Echem-SSPM which subsequently correspond to the sensor simulation, data collection, and data analysis sections of Figure 1.

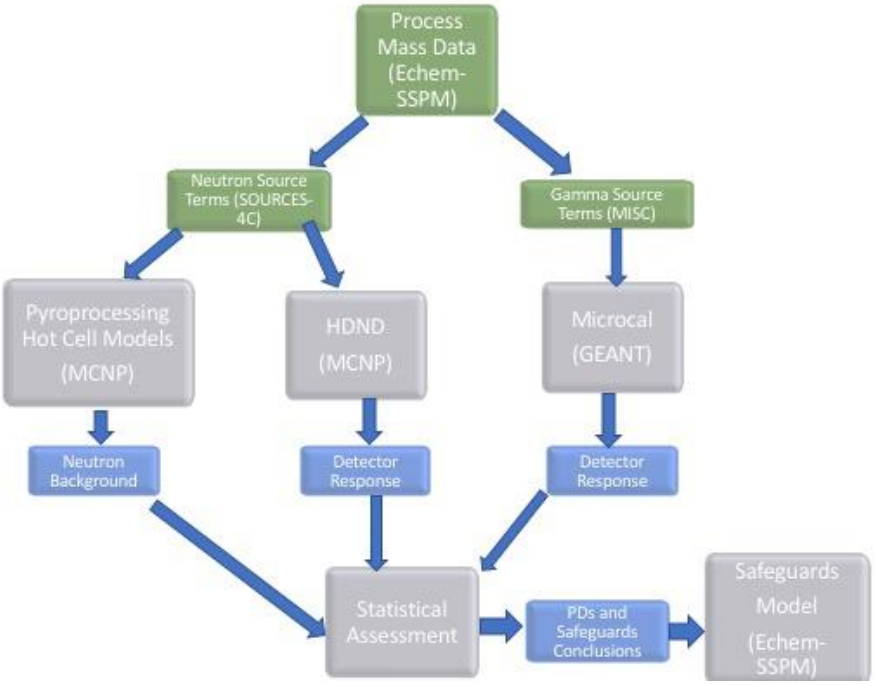

Figure 3. Flowsheet of advanced integration related models

This work utilized models of the detectors that had been previously developed and applied for the MPACT campaign as well as part of the detector development.[8,9] The goal of this work was not to improve the modeling of the measurements, but to improve on past work with regards to efforts related to advanced integration in the VFDTB. Past modeling work involved the application of the HDND for pyroprocessing signatures, statistical analysis of gamma signatures, as well as radiation maps of the process cell before and after the electrorefining separations step.[10,11,12] The past work was improved by utilizing updated data that accounted for isotopic rather than elemental composition that had been calculated using the safeguard flowsheet modeling in the SSPM. Additionally, more advanced geometry was developed to more accurately reflect the geometry and layout of process equipment in the process cell, and the scope was expanded in the case of the microcalorimeter to measure the U and U/TRU ingot response.

Monte Carlo N-Particle (MCNP) Models of the Pyroprocessing Hot Cell and the HDND

Modeling of the Pyroprocessing Hot Cell

The first of the simulation campaigns undertaken to develop results for advanced integration into SSPM were related to neutron background simulations and counting of the U ingot using the HDND in MCNP. The focus of the pyroprocessing hot cell modeling was specifically on the process cell of the pyroprocessing facility with no focus on the fuel fabrication cell or additional post-process storage cells. The process cell was developed utilizing information available from previous efforts in facility development and unit operations design using openly available sources.[13]

To model the facility, the flowsheet was simplified for the analysis and layout of the facility. A representation of this simplified flow sheet is seen in Figure 4. As seen in the flowsheet, the process cell was reduced to its core processes. The oxide reducer (OR), where the oxide fuel is processed to reduce the oxide fuel to metal, contains a neutron source from the anode basket placed within it during operation. The reduced fuel is transferred to the electrorefiner (ER) where it is processed, and U and U/TRU products are separated. Here, a source of neutrons takes several forms: the anode baskets and liquid cadmium cathode when operating as well as the salt always contains actinides in a near steady state thus contributing a constant source of background neutrons in the salt. The transferred product is then processed by the U and U/TRU processors to consolidate the U and U/TRU products to ingots and distill off salt and liquid cadmium products. The processors' consolidated dendrites, as well as distilled process salt, are notable neutron sources. Finally, the drawdown process was simplified into a single unit operation where the processed salt produces a neutron source in the process cell.

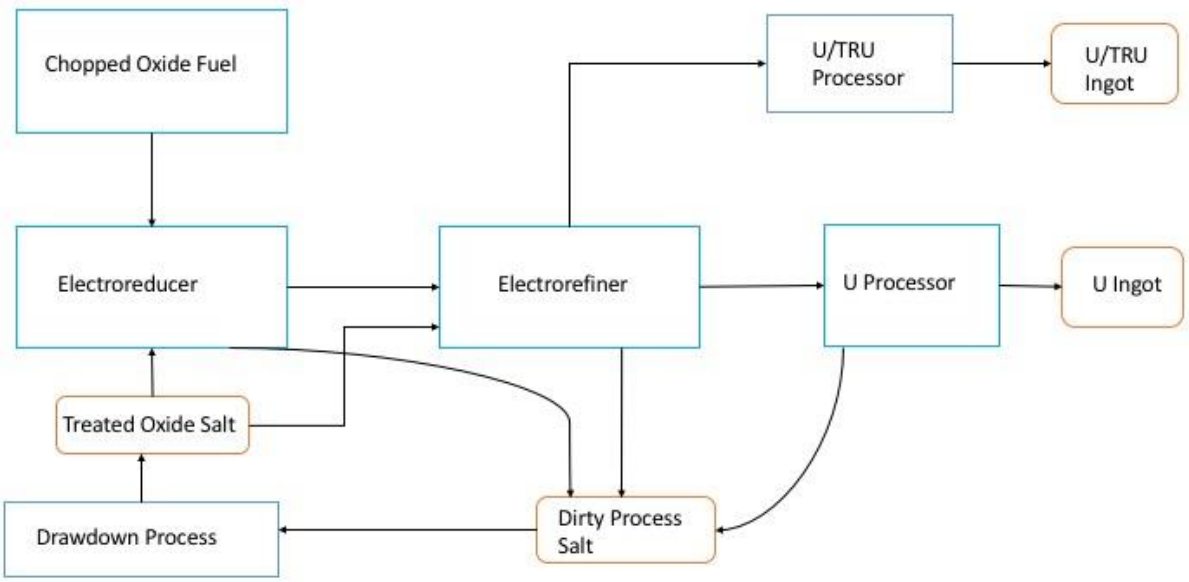

Figure 4. Simplified flowsheet for pyroprocessing process cell modeling

Modeling of Pyroprocessing Unit Operations and Hot Cell

The modeling in MCNP of the ER was notional and involved a series of fuel basket anodes. These electrodes were suspended in a LiCl-KCl bath in which U is periodically collected and removed for processing. The ER vessel that contains the salt and fuel baskets was a stainless-steel rectangular parallelepiped that contained the fuel baskets and eutectic salt. A visualization of this model is seen in Figure 5.

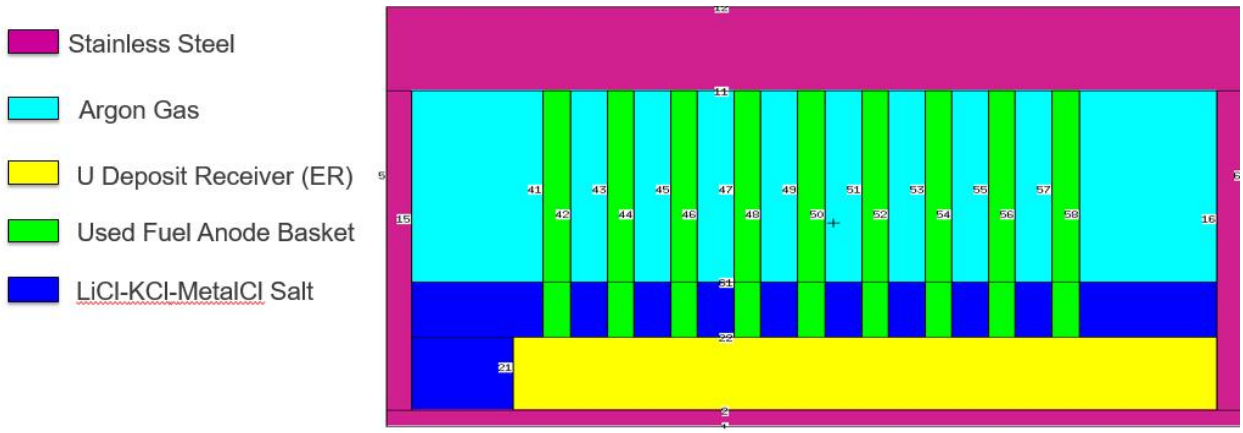

Figure 5. Electrorefiner MCNP model

The vessel of the U cathode processor (CP) was assumed to be made of steel and consisted of an inner and outer chamber to contain the heating elements of the inner chamber. The CP was modeled as having two crucibles. The crucible at the bottom and center of the inner chamber contains distilled salt and was made of stainless steel. Elevated above it on a tantalum platform was a second crucible made of graphite containing the U product. The crucible selected was based off a standard crucible that is able to contain the volume of U dendrites from the data provided from the SSPM. Between these two crucibles was a conical tantalum radiation shield. Each layer of steel for both the inner and outer chamber contained a thin copper lining. The atmosphere of the U CP was assumed to be argon like the rest of the hot cell. During a simulated CP operation, the graphite crucible contained the U product, and the steel crucible contained distilled ER salt. A visualization of this model is seen in Figure 6.

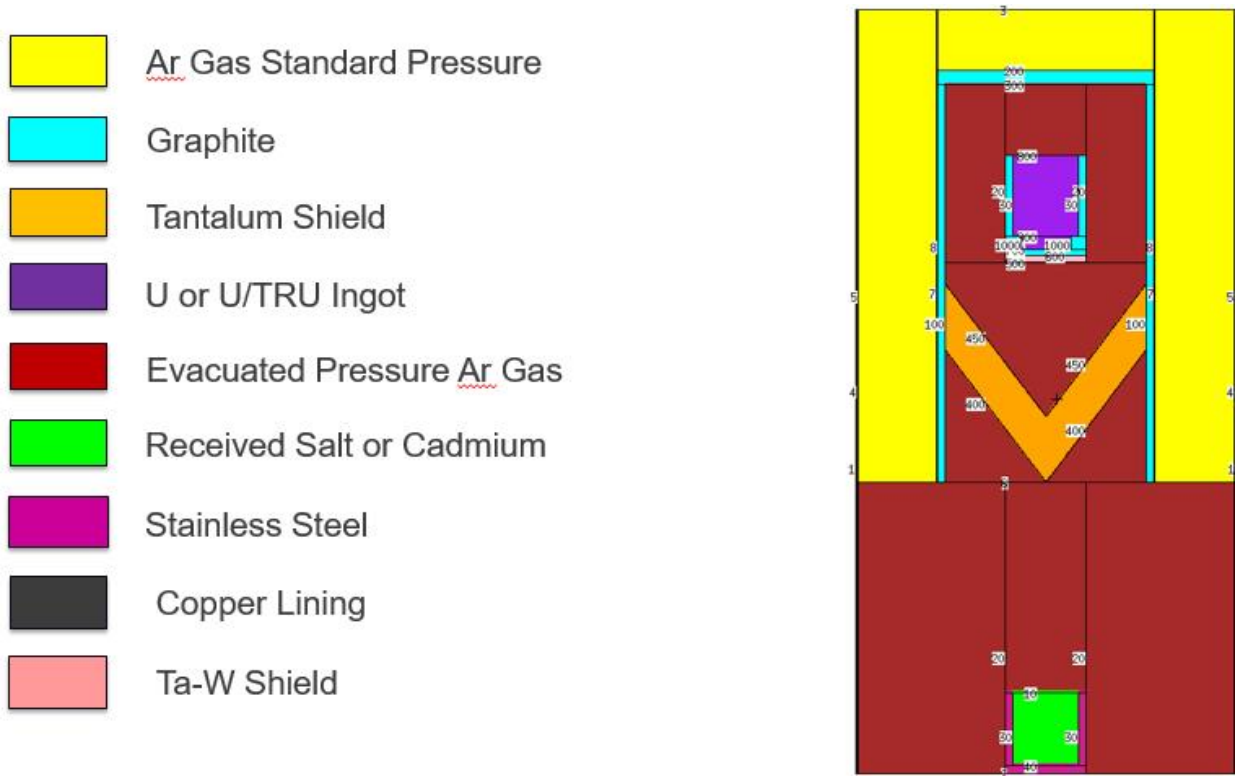

Figure 6. Cathode processor MCNP model

To model a notional OR, the geometry was assumed to be the same as that of the planar ER modeled before. The only difference being that the eutectic salt would not be LiCl-KCl but solely LiCl. The assumptions of the dimensions of the equipment were the same, consisting of planar baskets submerged in a eutectic salt with a rectangular parallelepiped serving as the vessel.

The U/TRU CP utilized the same geometry as the U CP. The difference being only what materials were present. Rather than ER salt being present in the lower receiving crucible, it instead contained liquid cadmium that has been distilled off from the crucible in the raised platform. The remainder of the dimensions and materials were identical to the U CP.

From the SSPM flowsheet, the pyroprocessing process consisted of four drawdown operations. These operations were the salt purification, oxidant production, U/TRU drawdown/ electrowinning, and fission product drawdown. These four processes were assumed to be combined in one process within the model. The notional drawdown equipment was modeled as an upright cylinder with the same assumptions for salt density and level as previously made for the ER. Due to the combination of several different processes, salt was always present in the process; however, it exists in different levels and masses depending on what drawdown steps are integrated.

The process cell was modeled integrating all of these individual unit operation models previously described. A drawing of the layout with the unit operations placed and labeled is seen in Figure 7. The process cell was assumed to be made of concrete enclosing an argon atmosphere.

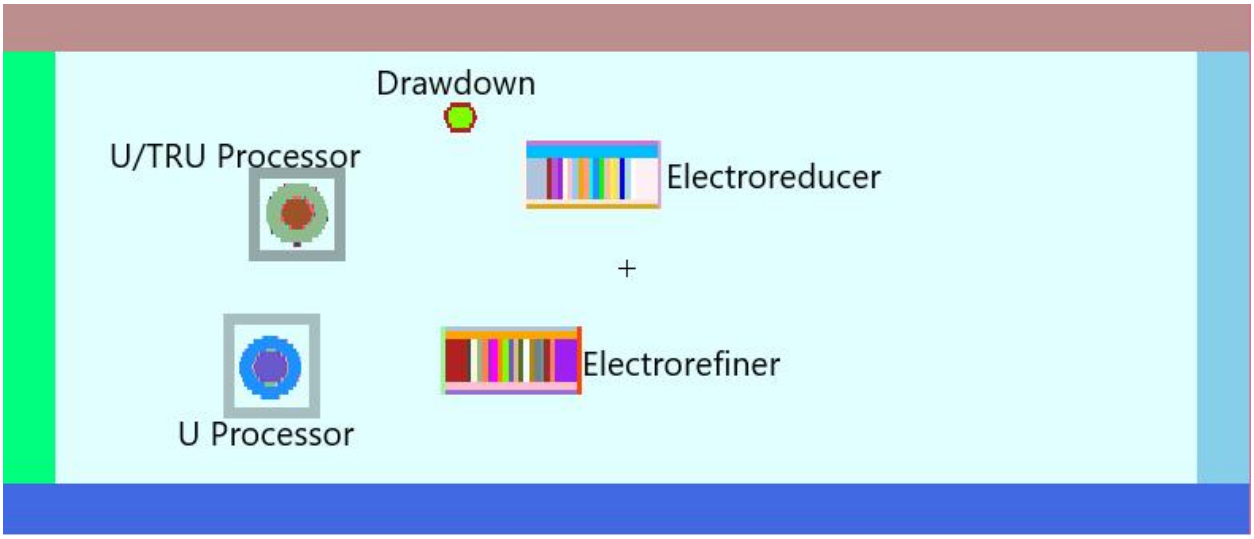

Figure 7. Notional layout of hot cell with unit operations in MCNP

Modeling of HDND

In addition to the modeling of the pyroprocessing hot cell in MCNP, the HDND was modeled in MCNP. The HDND allows for the counting of neutrons in high dose environments without the use of scarcely available Helium-3. The HDND consists of a rectangular filled array of parallel plates containing boron lined $Ar+CO_2$ filled tubes. There are a total of six of these parallel cells each about 0.5 centimeters thick and each layered with 1.6 cm thick plates of polyethylene to provide neutron moderation.[2] Neutron interactions with the boron produce charged alpha particles which are then registered in the gas. The detector, as it is modeled in MCNP, is seen in Figure 8.

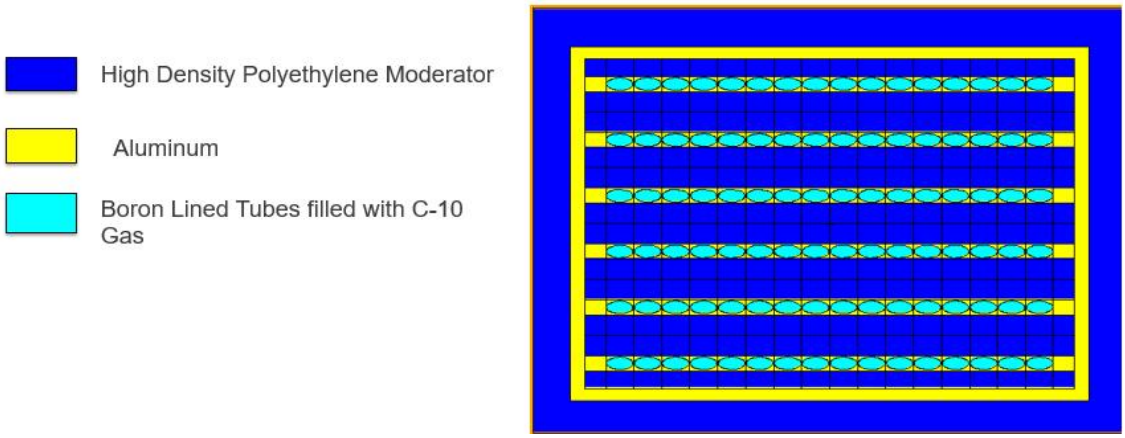

Figure 8. Top down view of HDND detector in MCNP

Determination of Source Terms

To apply these models of the pyroprocessing process cell and HDND detectors, applicable neutron source terms for the material in the process as well as the U ingot were modeled. Materials that move throughout the pyroprocessing hot cell produce radiation, especially neutrons. The source of these neutrons depends on the environment in which the source is being measured. Across all unit operations, where actinides are present there is a source of spontaneous fission neutrons, thus this source must be accounted for at all unit operations. In addition, due to the presence of LiCl and LiCl-KCl salts, especially their concentration of Li-7, the contribution of (alpha,n) neutron interactions as a source needed to be factored in. To calculate these source terms from both contributing sources, the software package SOURCES-4C was applied as it accounts for both sources of neutron emission.[4] To do this, the composition of each material of interest was read in and assumed to be homogenous. This composition was comprised of the major alpha emitters, spontaneous fission neutron emitters, and target isotopes such as Li-7 and Cl-32 that would be present to produce (alpha,n) reactions. With these compositions of the material, SOURCES-4C was used to calculate the spontaneous fission source, (alpha,n) source, and the total combined source as well as neutron energy spectrum for a selected number energy group between specified bounds. In addition to neutron source terms, source terms were calculated using MNCPTools to determine the gamma term utilizing MISC for the same composition of materials that were used to calculate the neutron source terms.[5,6] Both codes were selected because they allow for the easy integration of mass related data for isotopes from the material cards from MCNP developed for the materials in the process cell equipment and U ingot models.

Source Term Calculations: Movement of Material over Time

The material compositions for each unit operation in the pyroprocessing hot cell were calculated by the SSPM and provided a robust dataset of isotopic masses. Compositions were reported in hourly increments from 6300 to 6480 hours of operation, giving a 181-hour period under which the facility is assumed to be in steady state operation. A 31-hour snapshot of this period was taken between hours 6415 and 6445 to analyze material flow through the facility and the associated radiation signatures as a function of time and position. This specific period was chosen as it included operations from all relevant unit operations during this time. The amount of U/TRU present within unit operations fluctuated with time. When not in unit operations, material was either in storage awaiting processing outside the process cell, in movement within the hot cell, or in finalized ingots moved to storage in the fuel storage cells. The material was assumed to be adequately shielded in any of these three cases so that the only neutron flux present was contributed by material being processed in unit operations.

There was always a presence of U/TRU products in the ER salt. The OR anode was placed within the cell for the majority of this period, except for five hours of down time (6420-6424) where products were being transferred to the ER. The ER anode was inserted before the assessed time begins and was essentially exhausted of U/TRU material by hour 6433 where it was then removed and reinserted with new fuel to be processed at hour 6439. The liquid cadmium cathode (LCC) was also operated before the time assessed and increased in U/TRU content steadily until it was removed at hour 6433. The LCC is not in operation during the remainder of the time snapshot. Finally, the U and U/TRU CPs operated between hours 6433 and 6437. The presence

of TRU was greater in the U/TRU CP, though the total U/TRU mass is greater in the U CP, with the majority of it being U.

Neutron source terms were calculated for the pyroprocessing equipment's process materials using the time series data for each time between 6415 and 6445. These calculated source terms consisted of neutron intensity in terms of n/cm^3-s for both the spontaneous fission and (alpha,n) neutrons as well as energy distribution divided into 50 probabilistic bins between 0 and 10 MeV.

The majority of the neutron activity came from the ER salt and the salt drawdown (when it was operating). This was because of the increased level of (alpha,n) interactions due to the increased number of target isotopes in the salt as well as the high concentration of actinides, specifically significant masses of Cm. The ER anode source was not as significant due to a reduction in low-z target atoms as compared with the OR anode which produced neutrons at a greater rate than the ER anode before reduction operations had completed. The source terms for each individual unit operation followed the same trends as their U/TRU movement. With increased presence of U/TRU there was a correlated increasing neutron source.

The gamma source term was dominated by the fission products, specifically Cs-137, in the OR salt which makes up the majority of the gamma emissions calculated. Thus, the gamma source was a different consideration from that of the neutron background source since the majority of gamma emissions came from the OR as opposed to being spread out across the cell. Still, there are a significant amount of gamma emitters in the ER salt given that salt was the second greatest contributing factor to gamma emissions.

Background Radiation Flux Modeling

With the radiation source terms for the pyroprocessing process materials calculated, several modeling campaigns were then undertaken to determine the effects of radiation in the process cell and their affect and applicability from a process monitoring perspective. The first was the use of a flux mesh tally to measure the radiation fields of both neutrons and gammas produced by the calculated source terms.

Hot Cell Simulations: Neutron Flux FMESH Tallies

The first simulation campaign was to determine what the neutron flux profile throughout the cell was. This was performed via the application of an FMESH 4 tally with 250 equally spaced mesh elements in the x and y direction and one mesh element in the z direction which resulted in a total of 250^2 mesh points throughout the cell. Tallied fluxes in each grid element were presented in plotted form via MCPLOT. This simulation was performed for each time step between 6415 and 6445. Figures 9-13 provide the visual plots of these tallies.

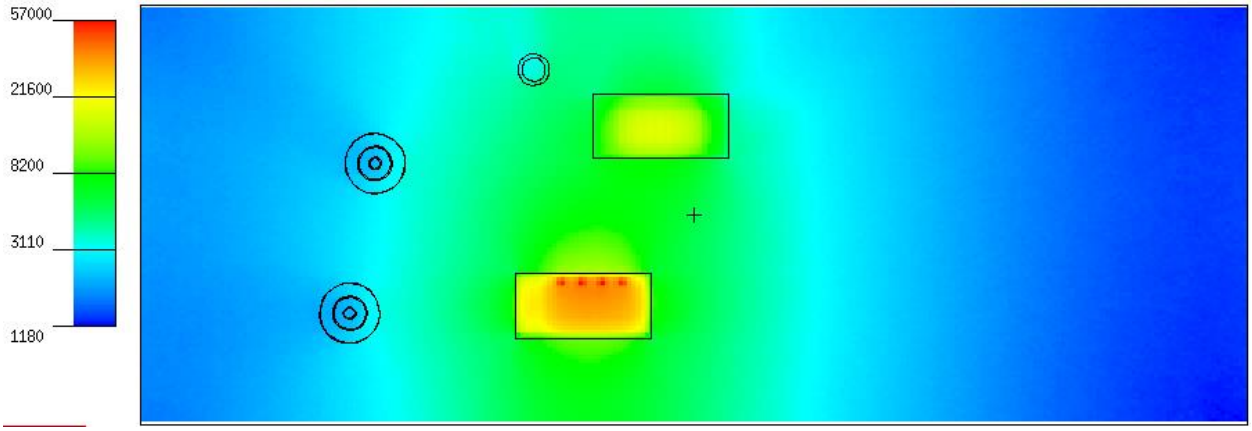

Figure 9. Neutron flux profile at time 6415 (n/cm^2-s). At this time, only the ER and OR were operating.

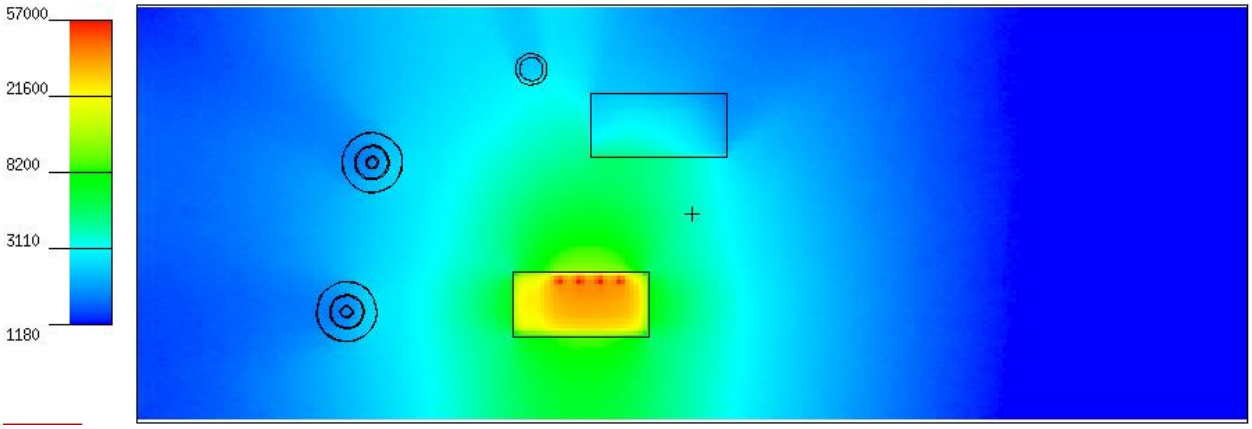

Figure 10. Neutron flux profile at time 6419 (n/cm^2-s). At this time, only the ER was operating.

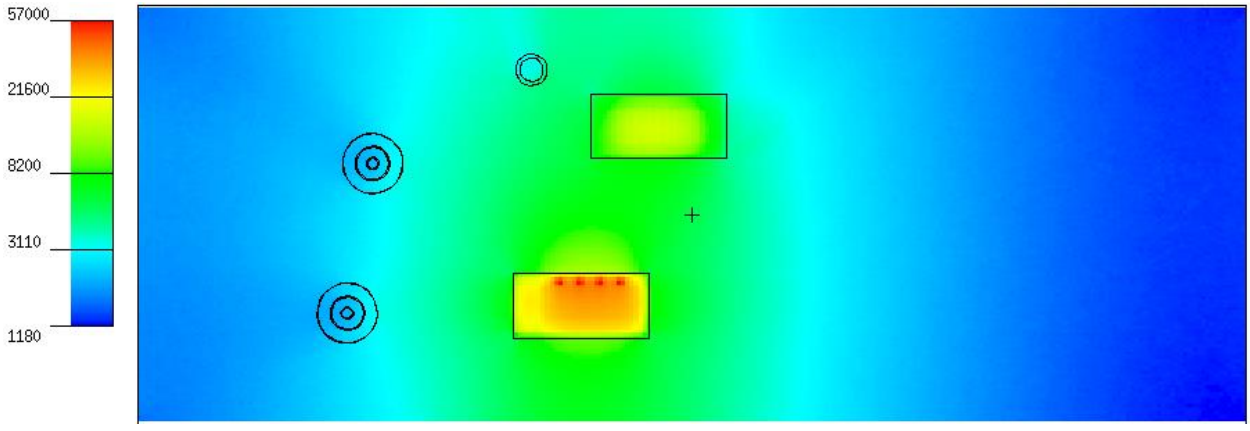

Figure 11. Neutron flux profile a time 6426 (n/cm^2-s), At this time, a new batch of fuel baskets had been placed in the OR for operating, and the ER was still operating.

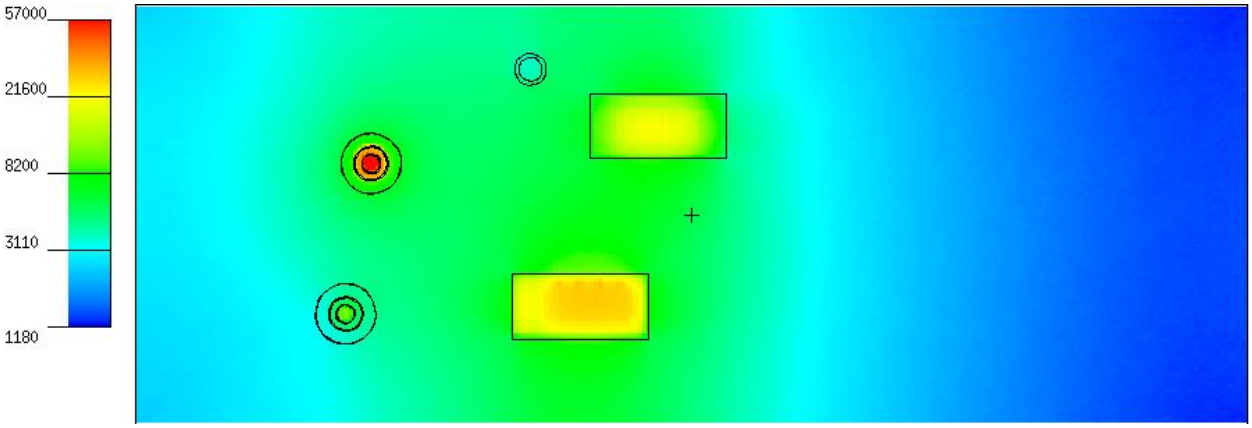

Figure 12. Neutron flux profile at time 6433 (n/cm^2-s), At this time, the U and U/TRU CPs were operating, the OR was reducing fuel, and the ER was having its anode fuel baskets removed.

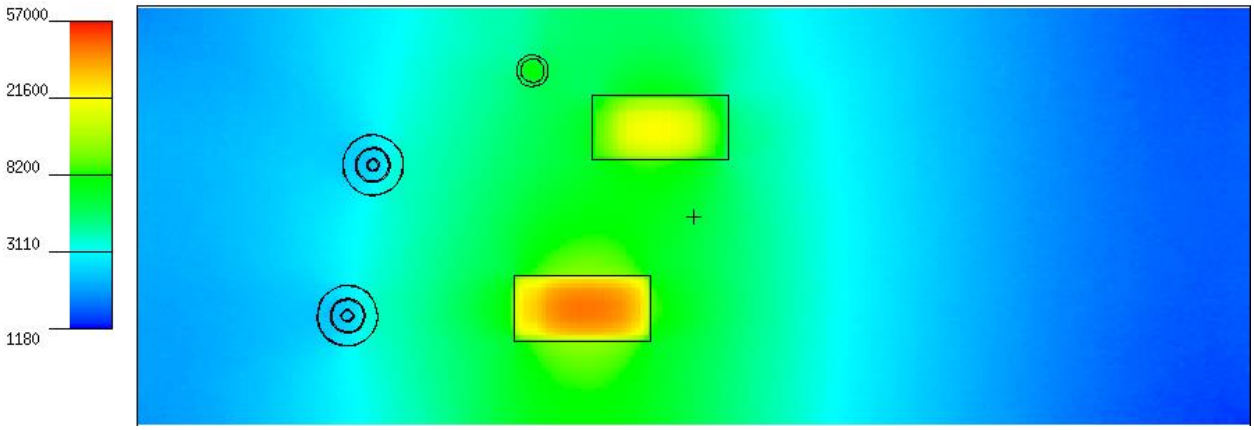

Figure 13. Neutron flux profile at time 6439 (n/cm^2-s). At this time, the drawdown processing canister was handling fuel, the ER was beginning to process fuel, and the OR was reducing fuel.

Beginning at time 6415, the neutron flux was dominated by the ER and the fuel baskets in the OR as expected. At time 6419, no substantial source was coming from the OR as the fuel baskets had been removed, while the salt in the ER still gave off the same strong source of neutrons. At time 6426, the reinsertion of the anode baskets in the OR resulted in the return of the source, though weakly, from the OR anodes. At time 6433, the U and U/TRU CPs were at the peak of their processing resulting in a noticeable flux coming from the processing equipment. At time 6439, the removal of the metal being processed was seen from the U and U/TRU CPs, and the collection of salt in the drawdown resulted in a noticeable, yet faint, source of neutrons from the drawdown equipment.

Hot Cell Simulations: Gamma Flux FMESH Tallies

Subsequent to the neutron flux profile simulation, the gamma flux profile was simulated. This was performed via the application of the same FMESH 4 tally, tallying photons, with 250 equally spaced mesh elements in the x and y direction and one mesh element in the z direction

which resulted in a total of 250^2 mesh points throughout the cell. This simulation was performed for each time step between 6415 and 6445. Figures 14-17 provide the visual plots of these tallies.

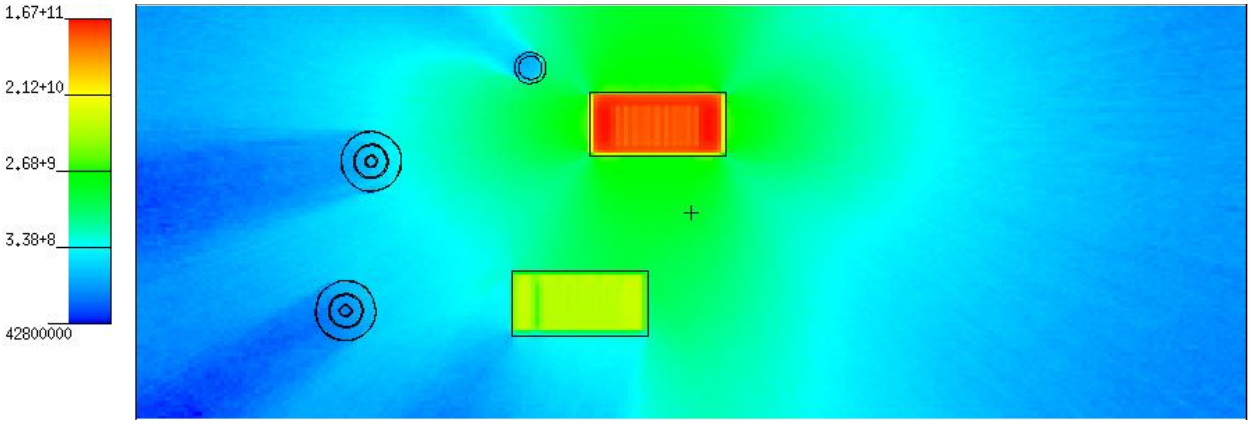

Figure 14. Gamma flux profile at time 6415 (gammas/cm^2-s). At this time, both OR and ER were processing fuel baskets.

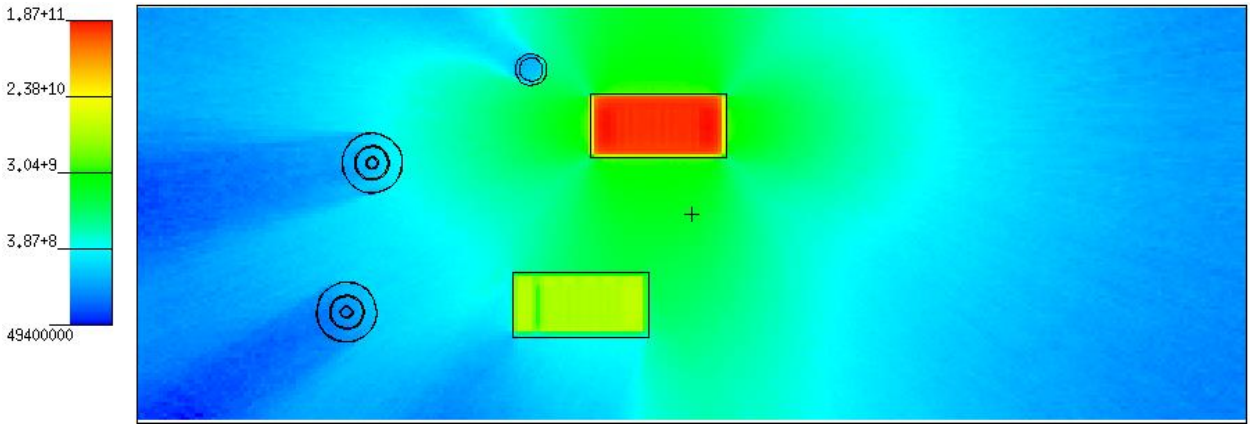

Figure 15. Gamma flux profile at time 6419 (gammas/cm^2-s). At this time, fuel baskets had been removed from the OR, and the ER was processing fuel.

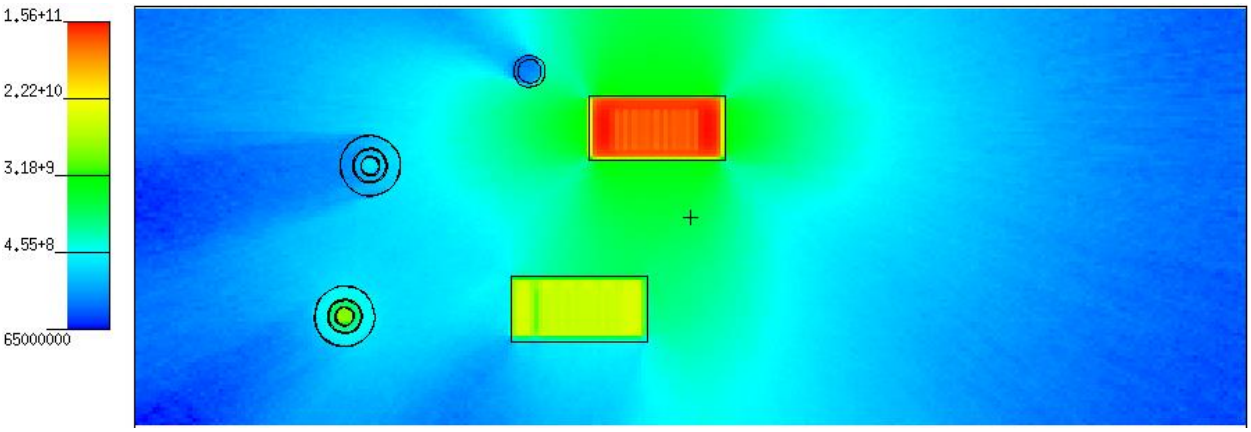

Figure 16. Gamma flux profile at time 6433 (gammas/cm^2-s). At this time, the OR fuel baskets had been replaced, the U and U/TRU CPs were processing their products, and the ER was having its fuel anode baskets removed.

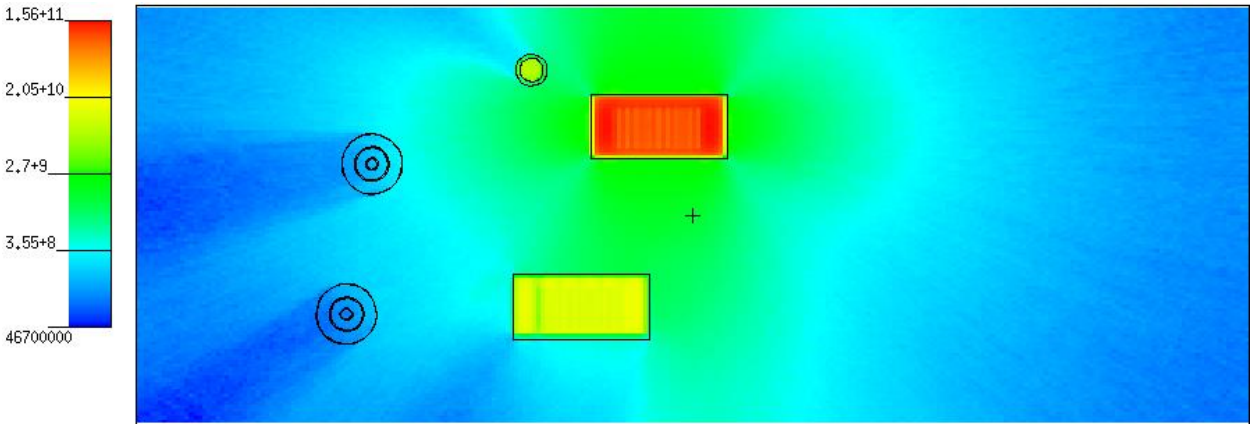

Figure 17. Gamma flux profile at time 6438 (gammas/cm^2-s). At this time, the OR and ER were processing fuel baskets, and the drawdown unit operations were processing salt.

For the entirety of the 6415-6445 time segment, the gamma source was dominated by the OR with a notable visible source from the ER due to presence of gamma emitters in the salt. At time 6419, with the removal of the OR fuel baskets, a gamma profile that encapsulated the whole of the OR was observed due to lack of internal shielding by the dense metal in the fuel baskets. At time 6433, like the neutrons, the operations of the U and U/TRU CPs were visible with the greater source of gammas coming from the U as opposed to the U/TRU CP indicating that the bulk of the gamma source was coming from the distilled ER salt containing the full range of fuel products. At time 6438, the operation of the drawdown and its resulting gamma flux was noticeable due to the presence of salt to be processed from both the OR and ER.

Hot Cell Simulations: Simulation of the HDND in the Hot Cell for Background Calculation

With the background calculated and characterized, the next effort was simulating the HDND inside of the hot cell to determine the magnitude of incident neutron background. This background was then integrated into the statistical analysis to determine how it effects the probability of detection of diversion. These simulations took several forms. The first was the simulation and calculation of the background neutron count rate. The second was the simulation of the gamma flux incident on the detector walls to derive information required for gamma effects on counting and electronics that could be discussed with the detector developers. Both of these campaigns are summarized in this section.

Hot Cell Simulations: HDND Background Counting Investigation

The HDND was placed at six different locations within the modeled hot cell to measure the neutron background. These locations were selected due to the range of proximity to unit operations and to provide a sense of the range of potential operating backgrounds throughout the hot cell and thus compare and select which location would be best and what shielding may be required to ensure proper counting of U and U/TRU products in-situ. A summary of these locations is shown in Figure 18 with each location numbered in relation to the hot cell.

The detectors utilized FT8 tallies in MCNP to register each individual capture of neutrons and subsequent alpha production. Results of these tallies were multiplied by the total emission rate to determine total background rate in the HDND in counts per seconds. The final results for the 31 different time cases at the six different positions are shown in Figure 19.

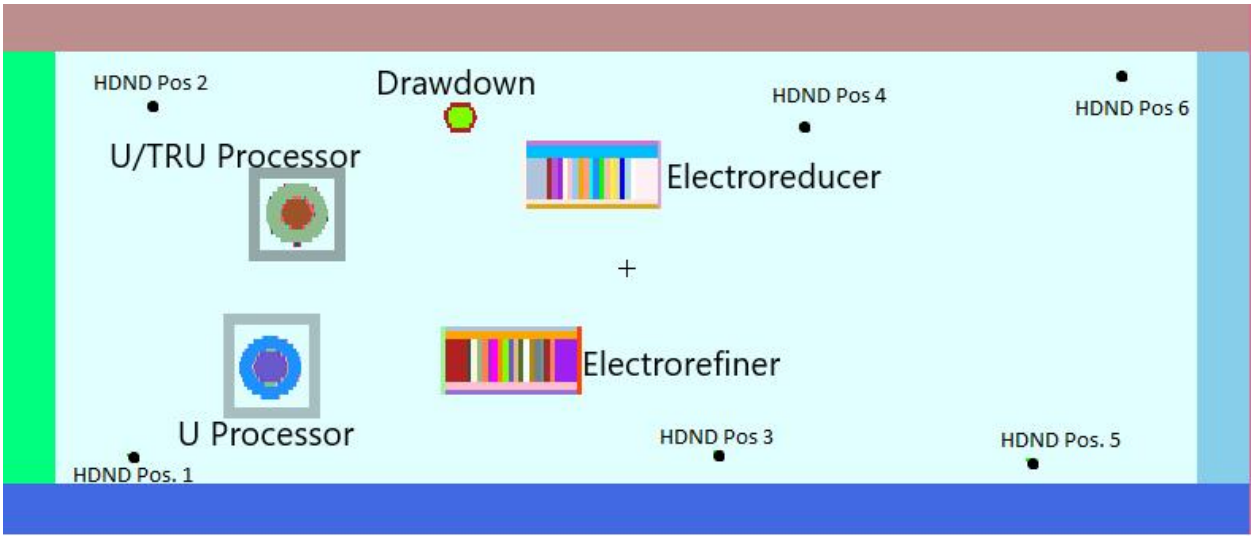

Figure 18. Modeled hot cell with position of detector indicated

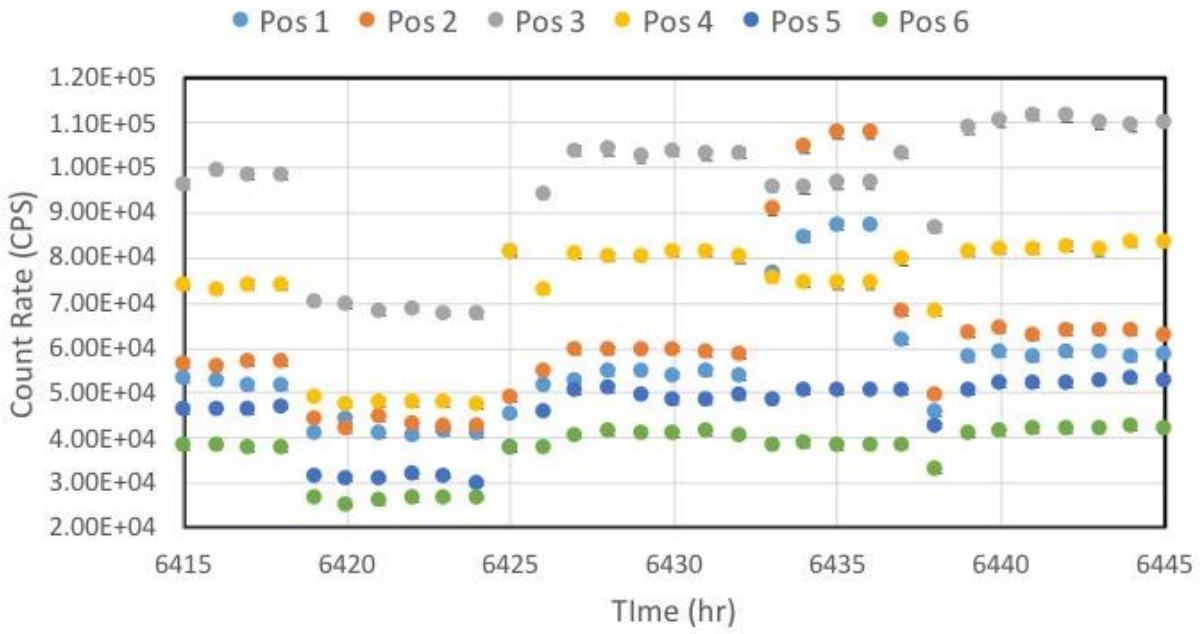

Figure 19. Weighted background neutron tally results

The results of these background calculations demonstrated several key takeaways. First, the greatest background count rates were present at positions 3 and 4 indicating that total number of background counts was related to the distance from the ER and the OR. As one might expect, the lowest background count rates came from positions 5 and 6 which were the furthest distance away from the processing equipment. This shows that for counting measurements to occur in cell, shielding the process equipment or an informed selection of detector placement will produce better counting conditions. Over the course of the 31 hours, the detectors followed similar trends. The counts for the first four hours were all around the same level. They then all subsequently dropped at time 6419 due to removal of fuel baskets from the OR. Upon the replacement of new fuel baskets in the OR, counts increased significantly in all detectors maintaining a similar rate until the U and U/TRU CPs were activated. When this occurred positions 3-6 saw a slight drop in counting rate due to removal of fuel baskets from the ER with the source from the U and U/TRU being a great enough distance away to be noticeable. For positions 1 and 2, however, there was a substantial increase in count rate as they registered the radiation from the processing equipment. After processing was completed, drawdown processing began and ER baskets were replaced, demonstrated by jumps in counting rates in positions 3-6 with decreases in positions 1 and 2 due to absence of a source from processing equipment.

Hot Cell Evaluation of Background Gamma Flux at the HDND Surface

To best evaluate the effectiveness of the HDND in the hot cell, an establishment of expected gamma flux was necessary as gammas can also deposit energy in the detector. This energy deposition will cause a count that is indistinguishable from a true neutron count, contributing to the observed background rate. Thus, studies were undertaken to determine the dose rate from

gammas at the surface of the HDND at all the previous designated positions. To do this, the flux was calculated at the surface of the HDND at all six detector positions using an F2 tally, and this calculated flux was then converted to a dose.

To summarize the results of this study, the gamma dose remained generally constant through the entire operation. It was dominated by the OR gamma source as expected. Thus, position 4 had the greatest dose due to being closest to the OR. The gamma dose increased with removal of the OR fuel baskets as the dense fuel material was not shielding the gammas being released by the fission products inside the OR salt. Reinsertions of fuel baskets led to a subsequent drop in dose. In addition, like the neutron source, positions 1 and 2 saw an increase in dose when the U and U/TRU CPs operated due to their proximity to the equipment—it was dominated by the presence of gamma emitters in the ER salt that is distilled off from the U product.

Next steps are to share the results of this gamma background study with the HDND team to determine the implications they will have on neutron counting efficiency in a hot cell environment.

Simulation of HDND Measurements of the U Product

With a neutron background count rate determined, simulations were then undertaken to measure a U product from the ER at all six detector positions in the presence of the background neutron radiation in the hot cell. These U ingots had a mass of 300 kg based off the size of the ingot from the updated data from the SSPM. This ingot was counted at various masses of Pu and U/TRU diverted from the U/TRU ingot to the U ingot. Advanced statistical methods were used to determine the probability of detection given a false alarm rate. This section explains the counts registered for both the standard U ingot and with material diverted from the U/TRU ingot. In addition, the analysis of the probability of detection with the statistical methods is documented.

Simulation of HDND Counting of U Ingots with Material Taken from U/TRU Ingot

The simulation campaigns of the HDND counts of the U ingot were undertaken to determine the effects on the counting rates for when Pu or bulk U/TRU is diverted from the U/TRU ingot and consolidated within the U ingot. This was expected to increase the neutron emission rate of the U ingot. Simulations needed to be performed to see the effect of the increased neutron emission rate on the HDND count rate of the ingot so that statistical testing could be applied to the difference in count rates to determine the probability of detection of Pu or U/TRU material in the U ingot. The counting occurred for a range of Pu and bulk U/TRU metal diverted from the U/TRU ingot to the U Ingot. For the Pu only case, these counting simulations assessed diversions between .005% to 1% by weight for diversion of Pu in the U/TRU into the U ingot. For the bulk U/TRU diversion, the counts were simulated for a range between .05% and 1% by weight of diversion of U/TRU to the U ingot. The diversion of Pu resulted in a range of contamination between .000059 wt% and .00012 wt% of the resulting U ingot. The diversion of the bulk U/TRU resulted in a range in contamination between .000073 wt% to .0015 wt% of the resulting U ingot. The results for count rates of the Pu only diversions at all six detector positions are seen

in Table 1. The results for count rates of the U/TRU diversions at all six counting positions are seen in Table 2.

Table 1. U ingot count rates with Pu from the U/TRU product

Weight Percentage of Pu in U Ingot	Pos 1 [CPS]	Pos 2 [CPS]	Pos 3 [CPS]	Pos 4 [CPS]	Pos 5 [CPS]	Pos 6 [CPS]
0	14.964	9.817	10.655	9.5151	11.275	10.218
0.000059%	15.349	10.054	10.898	9.7292	11.528	10.47
0.00012%	15.708	10.264	11.132	9.9462	11.73	10.682
0.00018%	16.01	10.523	11.449	10.216	12.138	11.013
0.00023%	16.419	10.698	11.642	10.378	12.325	11.182
0.00059%	18.341	12.126	13.19	11.737	13.922	12.637
0.0012%	21.892	14.318	15.643	13.953	16.585	15.01
0.0029%	32.12	21.105	22.901	20.493	24.35	21.986
0.0044%	41.081	26.944	29.297	26.185	30.871	28.078
0.0059%	49.552	32.626	35.386	31.656	37.578	34.015
0.0088%	66.991	44.008	48.041	42.797	50.864	46.147
0.012%	84.026	55.555	60.402	54.019	63.958	57.936

Table 2. U ingot count rates with U/TRU from the U/TRU product

Weight Percentage of U/TRU in U Ingot	Pos 1 [CPS]	Pos 2 [CPS]	Pos 3 [CPS]	Pos 4 [CPS]	Pos 5 [CPS]	Pos 6 [CPS]
0	14.964	9.817	10.655	9.5151	11.275	10.218
0.000073%	36.991	24.381	26.6461	23.562	27.905	25.356
0.00015%	58.752	38.877	42.397	37.763	44.687	40.482
0.00022%	80.495	53.519	58.138	51.775	61.421	55.6
0.00029%	102.58	67.802	73.804	65.612	78.006	70.624
0.00073%	235.12	154.92	168.5	150.54	178.19	161.43
0.0015%	529.03	347.61	377.99	337.67	398.96	361.91
0.0037%	1114.2	731.73	796.24	711.46	844.07	762.7
0.011%	3330.5	2178.5	2369.5	2115.7	2505.8	2268.1
0.015%	4444.1	2902.9	3166.7	2822.5	3343.2	3028.1

The results demonstrated several trends. The first was that the count rates for the U ingot with diverted bulk U/TRU was greater than that of the ingot with only Pu diverted. This is because the diverted U/TRU contained elements with high rates of spontaneous fission emission such as Cm and Cf. This also makes these count rates distinctly higher compared to a normal ingot. Advanced statistical tests can be performed on these differences in count rate to determine

probability of detection. The ingot with Pu only for small diversions (.000059 wt% -.00023 wt%) had very low emission rates as very little Pu is placed within them, along the lines of several grams of Pu in a 300 kg ingot of U. Thus, detection probabilities should be calculated and assessed for these specific cases. Like with the normal U ingots, the count rates of these U ingots contaminated with U/TRU material were affected by the positions that they are counted at due to albedo neutron effects.

Statistical Assessment of U Ingot Counting Results

Statistical tests to determine the probability of detection for diversion were applied to the count rates calculated in the U ingot counting simulations for all the listed percentages and positions from Tables 1 and 2. To explain this statistical analysis, observe the following example case for the count rates from the U ingot simulations. Counting measurements for the U ingot for 5 minutes at position 1 would result in a normal ingot count rate of 4489 pulses/300 seconds, while an ingot with .012 wt% Pu contamination in the U ingot would have a count rate of 25207 pulses/300 seconds. These pulse rates are notably different and would lead to indication of Pu in the U ingot.

Given these noticeable differences, assuming neutron counts can be modeled by a Poisson distribution, a Z-score test was an applicable statistical test to be applied to detect a difference in counts. The Z-score is the statistic shown in equation 1:

$$Z = \frac{observed - expected}{\sqrt{expected}} \quad (1)$$

Here “expected” is the no diversion mean count rate and “observed” is the measured count rate. If there is a diversion of Pu, the observed count rate will be larger than what is expected under normal operation, and the observed value of *Z* will be large. To quantify what constitutes a large observed count rate, the distribution of *Z* when there is no diversion needed to be calculated.

For the examples considered in this paper, if there is no diversion and the count time is at least 5 minutes, standard statistical theory can be used to show that *Z* would have an approximate (standard) Gaussian distribution with a mean 0 and variance 1. Quantiles of the standard Gaussian could be used to set a threshold to distinguish between typical no diversion count rates and unusual count rates. Choosing a particular threshold determines a process monitoring false alarm rate. For example, the 95^{th} quantile of the standard Gaussian is 1.645. If 1.645 was chosen as the threshold and there is no diversion then 95% of the time *Z* will be less than 1.645 and 5% of the time *Z* will be greater than the threshold, which implies the 5% false alarm rate.

For the example above with a five-minute count time and a .012 wt% Pu contamination in the U ingot, on average Z will be equal to 309. A value of 309 is highly unusual if there is no diversion (the 99.999^{th} quantile of a standard Gaussian is about 4.26). Either something extremely rare occurred or there was a diversion.

Note that the last equation above shows how count times influence *Z* and ultimately the probability of detection. For count time *T*, the Z statistic is defined by equation 2:

$$Z = \frac{\sqrt{T}(observed - expected)}{\sqrt{expected}} \qquad (2)$$

Clearly, as count time increases, the ability to detect a difference between observed and expected count increases.

Ideally, to estimate the probability of detection, many physical experiments would be performed where Pu was diverted in the electro-refining process. Then neutrons would be counted to see how often *Z* detected a significant difference. As this is not possible, simulations were used to estimate the probability of detection for various count rates and different backgrounds.

An algorithm was developed to estimate probability of detection (PD) for various count rates and background rates from the MCNP simulations. For the U product, any diversion of Pu will lead to an increase in count rates.

Results were compiled by applying this algorithm to the counting results from Table 1. Figure 20 shows the PD for .00059 wt% to .012 wt% Pu contamination in the U ingot due to diversion for various counting times at all six positions given a 5% false alarm rate.

As shown in Figure 20, the PD increased with increased counting time as is expected from the model assumptions. In addition, the PD decreased with increased background counting rates. In addition, positions 1, 5, and 6 had noticeably higher PDs specifically at lower levels such as .0029 wt% Pu contamination in the U ingot. This was a combination of low background and advantageous counting positions and rates, i.e. near the wall as observed in section 5, which leads to higher count rates. Thus, to increase probability of detection, selection of counting location and proper shielding are both of notable benefit for the increased detection of Pu diversion. Finally, in all cases where count time is greater than 5 minutes, the PD was calculated to be near 1 starting at .0059 wt% Pu contamination in the U ingot. Thus, the primary concern for detection would be the optimization of counting of the ingots to detect lower level diversions.

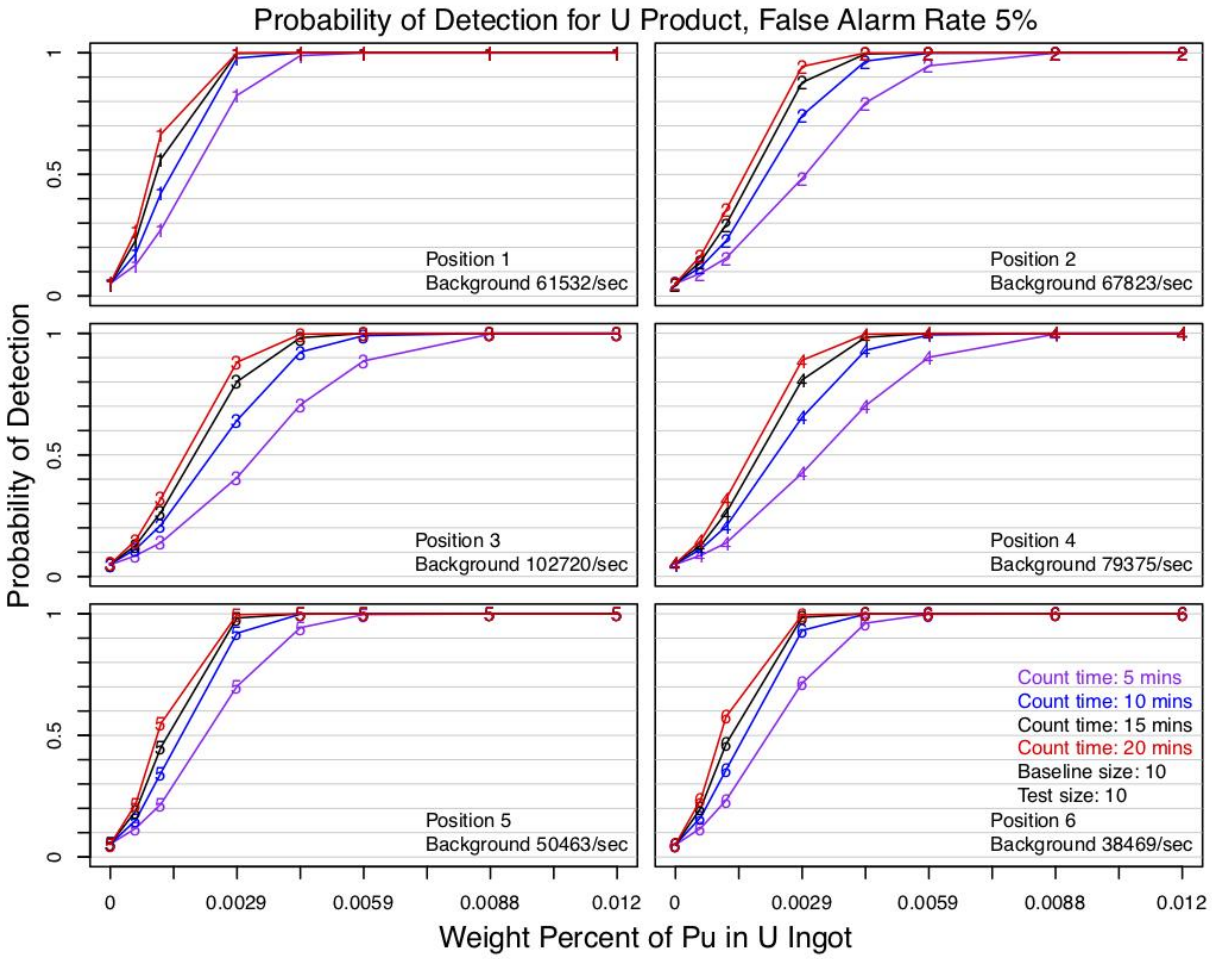

Figure 20. Probability of detection for the U product with Pu contamination (5% false alarm rate)

Simulation of the Microcalorimeter Detector for Gamma Signatures of the U Product Ingot

Simulated Gamma Microcalorimeter Spectrums

A subsequent statistical assessment was performed on the LANL microcalorimeter detector using the same material data for the U ingot composition. This was performed using a GEANT4 model of the microcalorimeter detector and the gamma spectra of the ingot using the MCNPTools MISC tool. The microcalorimeter is simulated in GEANT with the assistance of Rapid Adaptable Multi-threaded Particle and Radiation Transport Simulation (RAMPART) to control the simulations at the front end and to read in a GDML geometry file that had been applied previously in past microcalorimeter simulation campaign.[7,14,15,16] A visualization of the detector geometry is seen in Figure 21.

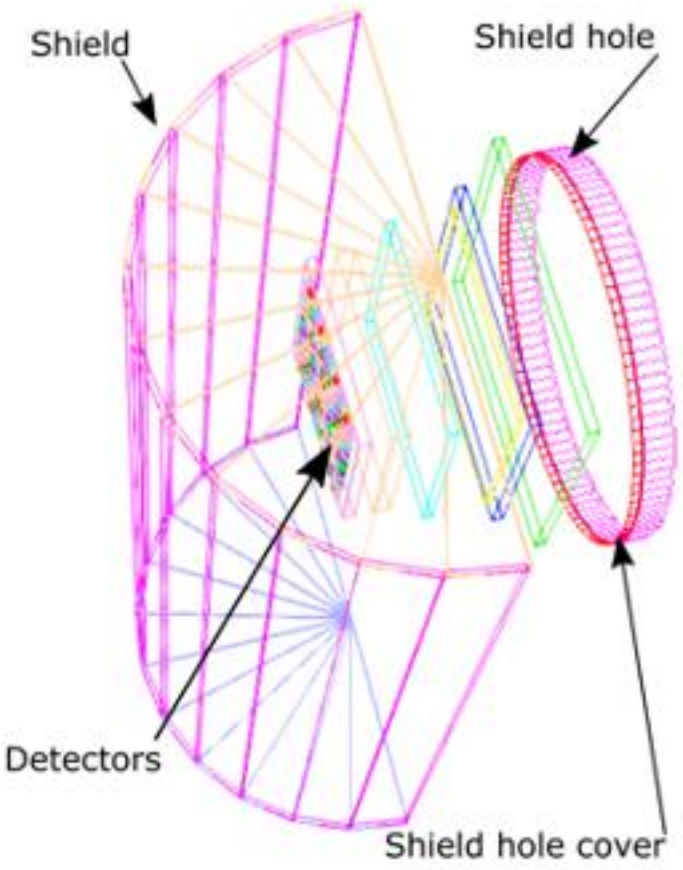

Figure 21. Visualization of the microcalorimeter geometry in GEANT

RAMPART stores statistics for each individual particle generated in the Monte Carlo simulation in a ROOT file whose statistics can be further assessed to produce a gamma spectrum.[17] This allows for the development of a response matrix that any calculated source spectrum can be applied to, rather than doing individual monte carlo simulations for each calculated source gamma spectrum. This has the benefit of significantly reducing the computational expense for simulating the microcalorimeter. For each particle, initial particle energy and deposited energy in the tin sensors are tabulated. Thus, histograms of intensity vs. deposited energy can be generated for every input energy in a set range. For this study, the input energy range consisted of a flat sampling spectrum of gammas between 0-3 MeV. This produced the histograms with intensities on a per particle basis. Each of these individual histograms for each input energy can be multiplied by the source intensity to generate a detector response for each energy of interest, and the summing of these products produces the total gamma spectrum. The source intensities for each gamma energy were calculated utilizing the MCNP isotopic source calculator previously described to produce the gamma profile of the hot cell. This method is described in depth in a primer produced during the modeling of the detector.[18]

Spectra were calculated for the U and U/TRU ingot. All spectra were produced in the form of per source particle basis and transformed to be in terms of a gammas/seconds*cm^3, as were the

subsequent statistical analyses. All simulations were performed for a 2π point source and did not take into account counting considerations such as self-shielding in the sampled material. The next sections detail the assessment method and application to the simulating counting response as it pertains to the U ingot spectra.

Statistical Assessment of Microcalorimeter Spectrum

A method was conceived for statistically assessing the gamma spectra to detect potential diversion of Pu and U/TRU from the U/TRU ingot to the U ingot.[8] The gamma spectra consisted of counts at N distinct energy bins. The counts in bin k were assumed to be independent Poisson random variables with mean $\lambda_k > 0$. For known λ_k, a new spectrum of counts can be simulated by drawing N independent Poisson (pseudo) random variables where the mean number of counts in bin k is λ_k. For example, if Y is the spectrum of counts that come from running the computer code, a new spectrum can be generated by treating Y as the mean spectrum and generating Poisson random variables with mean Y.

To explore possible relationships between off normal conditions and the ability to detect off normal, spectra were simulated from various off normal scenarios. For the comparison of the normal and off-normal counting spectrums the test statistic X^2 can be applied. Where X^2 is seen in equation 3 below:

$$X^2 = \sum_{k=1}^{N_e} \frac{(z_k - y_k)^2}{y_k} \quad (3)$$

Here N_e is the number of energy bins.

Recall that y_k is the count in energy bin k under normal operating conditions. Treating the spectrum Y as the true mean or, what is expected to be observed under normal operating conditions, then the test statistic has the form of equation 4:

$$X^2 = \sum_{k=1}^{N_e} \frac{(Observed_k - Expected_k)^2}{Expected_k} \quad (4)$$

This test statistic compares an observed count to an expected count under normal operation and then normalizes by the expected count. If the process is operating normally then X^2 will have a chi-square distribution with N_e degrees of freedom. A chi-square distribution with N_e degrees of freedom has a mean of m and a variance of $2m$. Crudely, if operations are normal then about 95% of the time X^2 will be less than $m + 2\sqrt{2m}$. If the process is off normal then X^2 will likely be larger than $m+2\sqrt{2m}$. How large X^2 is will depend on how different off normal is from normal and on the background. The approximate quantile $m + 2\sqrt{2m}$ is a threshold that determines the false positive rate. If the threshold is lowered, the false positive rate and the true detection rate are increased. If the threshold is raised, the false positive rate and true detection rate are both lowered. This test statistic is applied in the subsequent section to determine the probability of detection of diversion for various off-normal conditions.

U Ingot Assessment

Figure 22 shows simulated sums of counts, *Y*, for 5-minute count time for the normal, .00059 wt%, and .0012 wt% Pu contamination in U ingot simulations. The vertical dashed line in each plot is the 99th quantile of the normal data. For the .00059 wt% data, about 99% of the *Y* values were above (to the right of) this threshold (dashed line), and for the .0012 wt% data all of the *Y*'s were above the threshold. Figure 23 and Figure 24 shows similar results but for 10 and 20-minute count times, respectively.

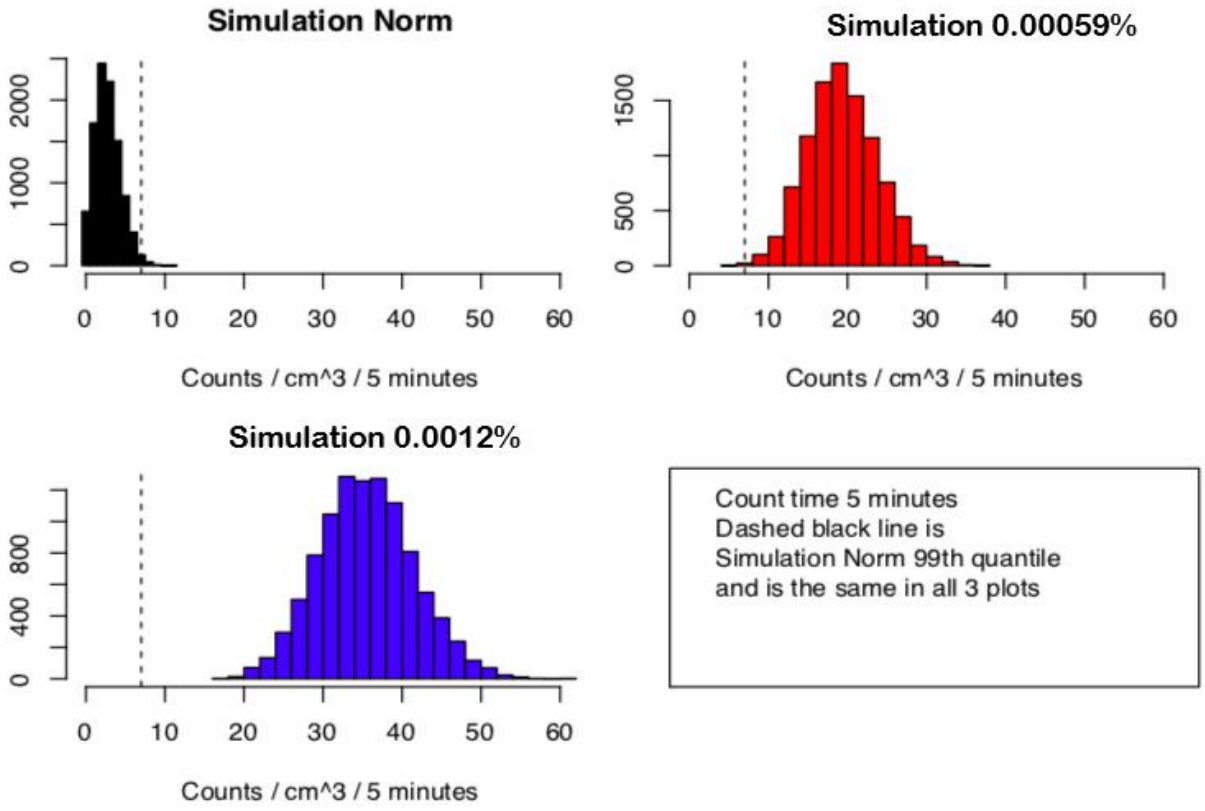

Figure 22. U ingot histogram of counts for 5-minute count time.

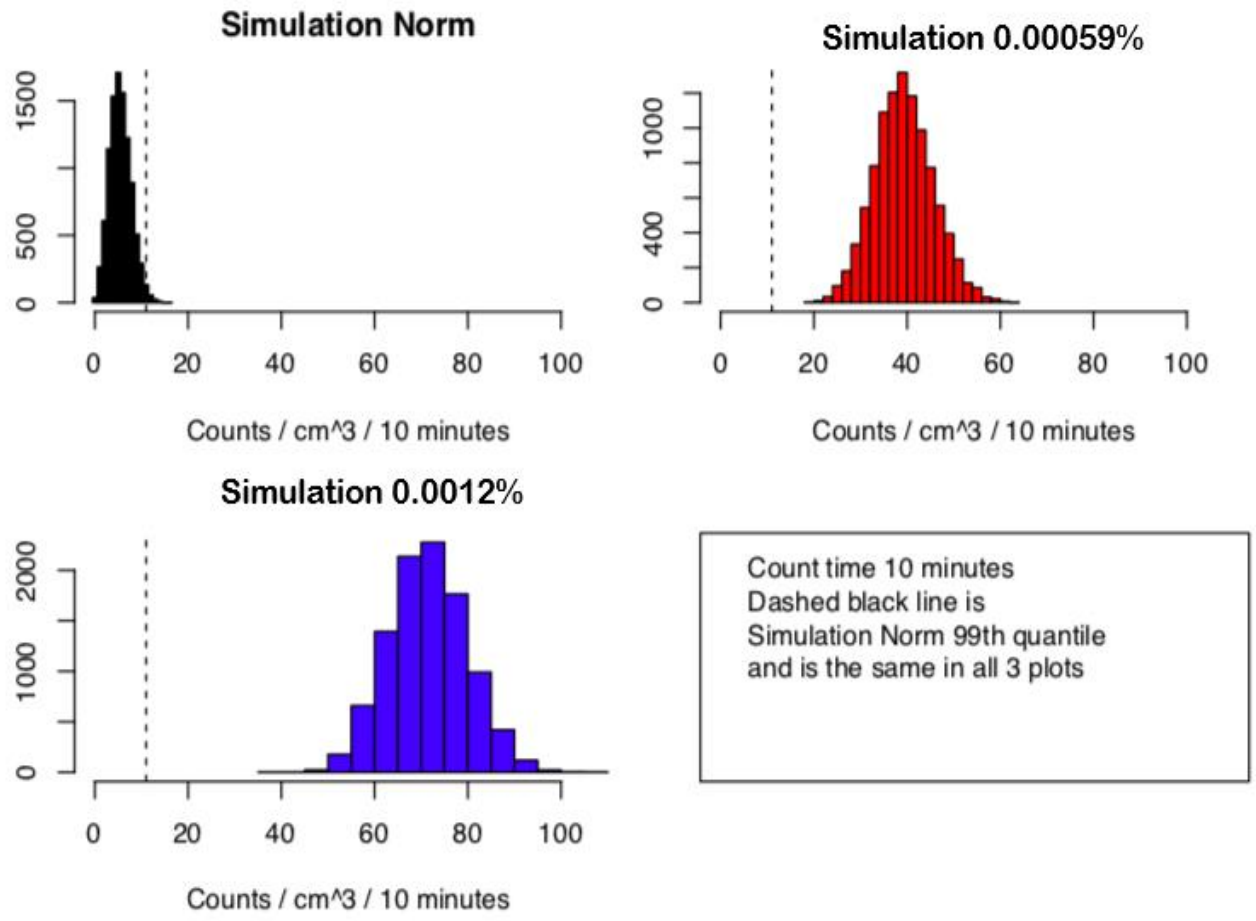

Figure 23. U ingot histogram of counts for 10-minute count time.

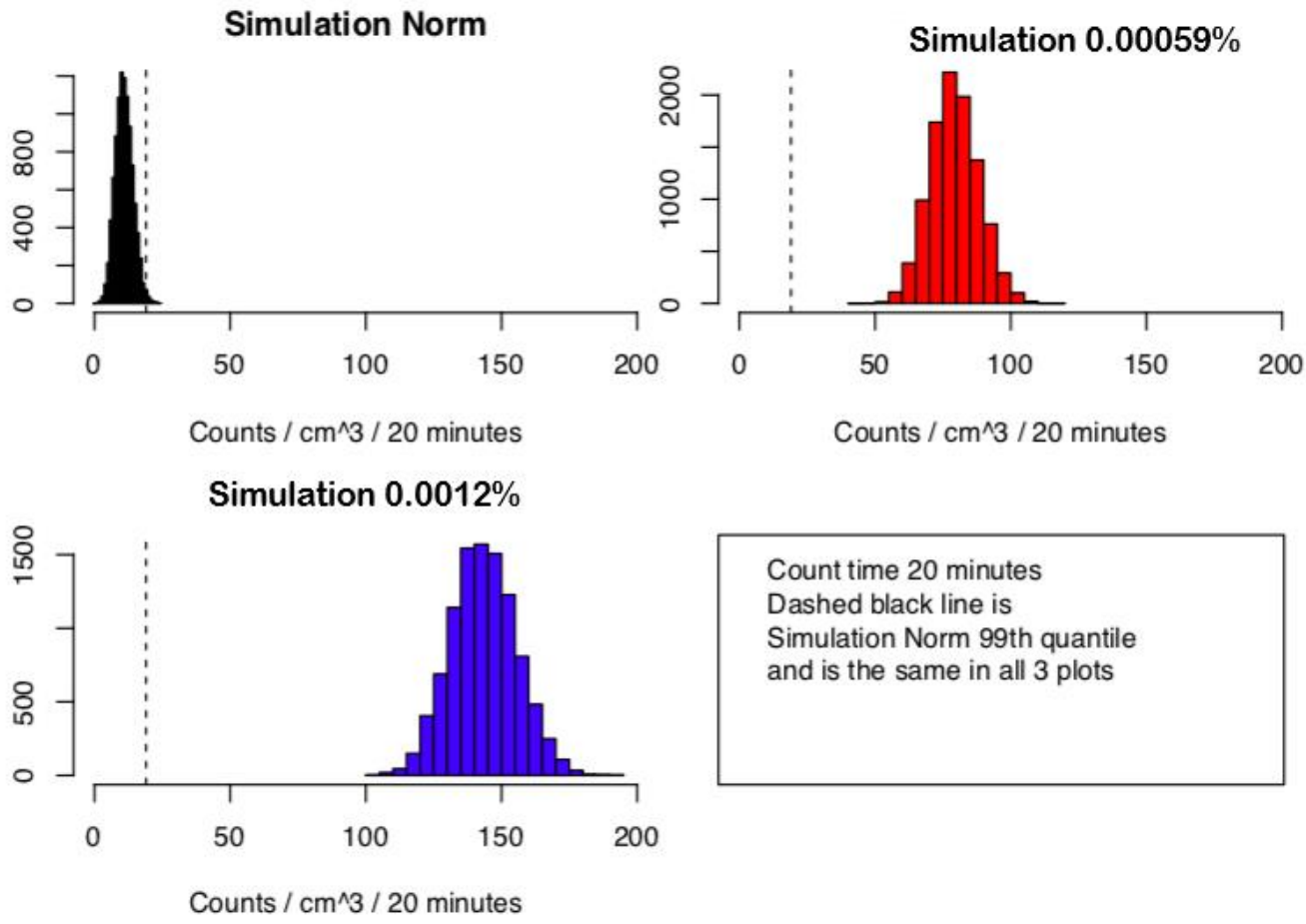

Figure 24. U ingot histogram of counts for 20-minute count time.

It can be concluded from these results that with at least 20 minute count times and counts in 19 energy bins, the distribution of counts for a normal operating environment was approximated reasonably well by a Gaussian distribution, and there is a probability of detection of at least 0.99 for levels of Pu contamination, due to diversion, as small as 0.00059 wt% Pu in the U ingot for a false alarm rate of 1%.

Conclusions

Multiple models were developed for the advanced integration of safeguards measurements into the Milestone 2020 VFDTB. Utilizing data from the VFDTB's safeguards model, SSPM, the pyroprocessing hot cell and its associated safeguards measurements in MCNP were modeled. The model of the hot cell demonstrated that there are noticeable changes in flux over time at different locations in the hot cell. The dominant source is from the used fuel baskets and the ER salt which contributes both a large number of spontaneous fissions and alpha-n neutron reactions.

The presence of neutron emitting material in unit operations and their movement between them can be potentially monitored using deployed HDNDs or other neutron monitors, as modeled detectors exhibited noticeable responses to changes in material movement in the hot cell.

The modeling of the HDND to detect the presence of Pu demonstrated that neutron counts even in the presence of high neutron background were able to detect the presence of small amounts of Pu in the U product ingot. The statistical methods used were able to detect the presence of Pu as low as 0.0059 wt% contamination of a 300 kg U ingot with a high PD of .9981 with counting times as low as 5 minutes assuming the counts are performed away from the ER and other unit operations. With increased counting times and lower incident neutron background, the PD increased. A table of the PDs for various counting times and Pu contamination of the U ingot calculated at the detection position 6 furthest away from the unit operation equipment, and thus least incident background, is seen in Table 3. It is important to note that these probabilities are based off the specific measurement case of our analysis. The results do not take into account factors such as detector dead time as well as effects of incident gamma radiation on the HDND. These probabilities are demonstrably high and can be integrated into the measurement section of the SSPM model, but should not be taken as absolute PDs as there would be a likely reduction in this value if factors such as detector dead time and incident gamma were accounted for.

Table 3. Probability of detection at detector position 6 away from the unit operations equipment

Weight Percentage of Pu in U Ingot	5 Minute Count Time [PD]	10 Minute Count Time [PD]	15 Minute Count Time [PD]	20 Minute Count Time [PD]
0.00059%	.1189	.1636	.2016	.2635
0.0012%	.2333	.3585	.465	.5774
0.0029%	.715	.9316	.9856	.9959
0.0044%	.9615	.9981	1	1
0.0059%	.9981	1	1	1
0.0088%	1	1	1	1
0.012%	1	1	1	1

Similar analysis to detect Pu diversion in the U ingot utilizing the microcalorimetry detector was also undertaken. This analysis showed that the microcalorimeter could be used to detect the presence of Pu, but the counting time required was not optimal as longer count times (20-40 minutes) are required to ensure that the shape of the spectra is not skewed to apply the test statistic. This demonstrated that for detection of Pu in the U product, neutron counting should be the selected approach.

The next step for advanced integration is to take these probabilities as well as conclusions about the nature of radiation background and integrate the PD results into the SSPM for its key measurement points, shown in Figure 2, to determine the impact on inventory difference and standard error of inventory difference. In addition, the background radiation results and radiation map are to be integrated into the physical layout model to help inform conclusions regarding physical security.

KEYWORDS: Safeguards; Advanced Integration; Pyroprocessing; Measurement Simulations; NDA

AUTHOR BIOGRAPHIES

Philip Lafreniere is a Postdoctoral Research Associate in the Nuclear Engineering and Nonproliferation Group, NEN-5 at Los Alamos National Laboratory. He earned his BS, MS, and PhD in Nuclear Engineering from the University of New Mexico.

Mike Fugate is a Scientist 3 in the Statistical Sciences Group, CCS-6 at Los Alamos National Laboratory. He earned his BS, MS, and PhD in mathematics from the University of New Mexico.

Brian Key is a Deputy Group Leader in the Nuclear Engineering and Nonproliferation Group, NEN-5 at Los Alamos National Laboratory. He earned his BS and MS in Chemical Engineering at the University of New Mexico.

References

1. Cipiti, B.B. et al. 2012. Modeling and Design of Integrated Safegaurds and Security for an Electrocehmical Reprocessing Facility, SAND2012-9303, Sandia National Laboratories.

2. Henzlova, D. and Menlove, H. 2017. High-Dose Neutron Detector Development for Meausring Alternative Fuel Cycle Materials, *Proceeding of Global 2017*, Seoul, South Korea.

3. Hoover, A. et al. 2016. Progress, Performance, and Prospects of Ultra-High Resolution Microcalorimeter Spectrometrers, LA-UR-16-26714, Los Alamos National Laboratory.

4. Wilson, W. et al. 2002. Sources 4C: A Code for Calculating (alpha,n) Spontaneous Fission, and Delayeed Neutron Sources and Spectra, LA-UR-02-1839, Los Alamos National Laboratory.

5. Solomon, C. 2012. MCNP Intrinsic Source Constructor (MISC): A User's Guide, LA-UR-12-20252, Los Alamos National Laboratory.

6. Solomon, C., Bates, C., and Kulesza, J. 2017. The MCNPTools Package: Installation and Use, LA-UR-17-21779, Los Alamos National Laboratory.

7. Agostinelli, S. et al. 2003. Geant4-A Simulation Toolkit, *Nuclear Instruments and Methods in Physics Research A*, Vol. 506, pp. 250-303.

8. Tutt, J.R., Fugate, M.L., and Key, B.P. 2018. Advanced Integration of High Dose Neutron, Micorcalorimeter, and Voltammetry Sensor Technologies in an Electrorefining Process, LA-UR-18-29076, Los Alamos National Laboratory.

9. Hoover A. S. *et al*., 2009. Application of GEANT4 to the Simulation of High Energy-Resolution Microcalorimeter Detectors, *IEEE Transactions on Nuclear Science*, Vol. 56, No. 4, pp. 2294-2298.

10. Durkee, J.W. 2018. Simulated Time-Dependent HDND Radiation Signatures and Radiation Movies for Pyroprocessing Using MCNP6, LA-CP-18-20159, Los Alamos National Laboratory.

11. Fugate, M.L., Key, B.P., and Tutt, J.R. 2019. Monitoring an Electro-refiner Process Revision 1, LA-UR-19-29553, Los Alamos National Laboratory.

12. Durkee, J.W. 2012. Characterization of Delayed-Neutron and Delayed-Gamma Pyroprocessing Emission Signatures Using MCNP6, LA-UR-12-25807, Los Alamos National Laboratory.

13. Chang Y.I. et al., 2018. Conceptual Design of a Pilot-Scale Pyroprocessing Facility, *Nuclear Technology,* Vol. 00, No. 1, pp. 1-19.

14. Allison, J. et al. 2006. Geant4 Developments and Applications, *IEEE Transactions on Nuclear Science,* Vol. 53, No. 1, pp. 270-278.

15. Allison J. et al. 2016. Recent Development in Geant4, *Nuclear Instruments and Methods in Physics Research A,* Vol. 835, pp. 186-225.

16. Budden, B.S. et al., 2018. SABRS GRESS Environment: User and Developer Guide 2018 Edition Buddem, LA-CP-18-26073, Los Alamos National Laboratory.

17. Tanabashi, M. et al., 2018. Review of Particle Physics, *Phys. Rev D,* Vol. 98, 030001.

18. Esch, E. 2020. Creating a Detector Response Matrix for Micro-Calorimeter, LA-UR-20-25876, Los Alamos National Laboratory.